ESD-TR-71-116

Technical Note

1971-11

C. W. Frasier

Seismic Scaling of Explosive Source Functions Using Teleseismic P Waves

14 April 1971

Prepared for the Advanced Research Projects Agency
under Electronic Systems Division Contract F19628-70-C-0230 by

Lincoln Laboratory
MASSACHUSETTS INSTITUTE OF TECHNOLOGY
Lexington, Massachusetts

Approved for public release; distribution unlimited.

MASSACHUSETTS INSTITUTE OF TECHNOLOGY

LINCOLN LABORATORY

SEISMIC SCALING OF EXPLOSIVE SOURCE FUNCTIONS USING TELESEISMIC P WAVES

C. W. FRASIER

Group 22

TECHNICAL NOTE 1971-11

14 APRIL 1971

LEXINGTON MASSACHUSETTS

The work reported in this document was performed at Lincoln Laboratory, a center for research operated by Massachusetts Institute of Technology. This research is a part of Project Vela Uniform, which is sponsored by the Advanced Research Projects Agency of the Department of Defense under Air Force Contract F19628-70-C-0230 (ARPA Order 512).

ABSTRACT

Short period P waves of four presumed Soviet explosions from Eastern Kazakh are examined at five teleseismic arrays: LASA, YKA, OONW, WRA and GBA. Transfer functions to shape the lower magnitude to the highest magnitude event were computed at each array to eliminate transmission path effects from source to receiver. The transfer functions are locally consistent from sensor to sensor at each array, but show considerable global variations from array to array. This suggests that there are strong azimuthal variations in the source radiation of the events, due to complex scattering of the signals at the test site. At LASA, the observed transfer functions can be explained by using explosion source functions of Blake and Haskell. The assumed source parameters are scaled functions of the yield of each event, which is estimated from an empirical amplitude yield relationship.

Accepted for the Air Force
Joseph R. Waterman, Lt. Col., USAF
Chief, Lincoln Laboratory Project Office

I. INTRODUCTION

In a previous Technical Note, Filson[1] discussed the short period spectra from five presumed nuclear explosions from Eastern Kazakh recorded at five world wide arrays. His analysis consisted in fitting the corrected displacement spectrum of each event at each array to a scaled explosion source model given by Haskell. In order to use the observed data, corrections had to be made for instrument response, crustal and mantle layering, and average attenuation effects in the Earth. In spite of the uncertainties in estimating these quantities, Filson was able to demonstrate a systematic shift of the displacement frequency content towards lower frequencies with increasing magnitude as predicted by Haskell's explosive source model.

In this report a different technique is used to verify the apparent seismic scaling effect with magnitude found by Filson. Using four of the events analyzed by Filson, transfer functions are computed in time which shape each of the lower magnitude events to the largest event at each array. For each pair of events this is equivalent to taking the spectral ratio of the largest P wave over a smaller P wave, both recorded at the same site. Such transfer functions cancel out all the unknown transmission path effects and the instrument response at each site, and therefore can be interpreted as spectral ratios of the source radiations of the events.

In computing transfer functions at a given array, one can use either the data from individual sensors or steered beams for the entire array. Whereas steered beams generally have better signal to noise ratios than signal sensors, the self-consistency of the data can be tested by computing transfer functions at each sensor. If such functions are coherent across the entire array, then they can be reliably interpreted in terms of

source functions. The first part of the data analysis shows that quite consistent transfer functions are obtained in the individual sites of each array, in spite of large fluctuations of signal shape and amplitude. Thus no apparent differences in radiation patterns can be detected within each array.

Array beams of each event are shown in the second part of the data analysis. Transfer functions are computed from this data at each array. For reasons described in that section the LASA transfer functions are considered most reliable for interpretation in terms of source functions.

Two sets of source functions are calculated for the events, using models given by Haskell and Blake. Yields for the four events are estimated from an empirical magnitude-yield formula for explosions in hard rock. From the yields the Haskell and Blake solutions are obtained by scaling the yield dependent parameters.

Finally, theoretical transfer functions are computed from the two sets of source functions, and they are compared to the LASA transfer functions.

II. DESCRIPTION OF DATA AND ARRAYS

The short period data used in this analysis was recorded at five arrays azimuthally distributed about the Soviet test site in Eastern Kazakh. These arrays are the following: (LASA), the Large Aperture Seismic Array in Montana, USA; (GBA), near Gauribidanur, India; (WRA), near Warramunga, Australia; (YKA), near Yellowknife, Canada; and (OONW) near Oslo, Norway. In Figure 1 the location of each array is shown relative to the Soviet test site denoted here by (STS). The epicentral distance from the test site to each array varies from $\sim 36^{\circ}$ at OONW to $\sim 89^{\circ}$ at WRA.

The geometries of the arrays are shown in Figures 2 and 3. Clearly LASA, with an aperture of 200 km. is an order of magnitude larger than the other arrays. GBA, YKA and WRA are arrays operated by the United Kingdom, and OONW was a temporary array set up by the United States, but now not operating. These smaller arrays each consist of two orthogonal arms of evenly spaced seismometers, the arms being 20 km. long or less.

The short period displacement response of the seismometers contained in the arrays is shown in Figure 4. Converting these two curves to velocity response one obtains a curve for LASA and UK which is flat from about 1 to 4 Hz and an OONW curve which is flat from about 1 to 2 Hz tapering off slowly above 2 Hz.

These first four figures are taken from Filson's report.[1]

The data consists of the short period teleseismic P waves from four presumed explosions from Eastern Kazakh recorded at the arrays described above. Table 1 is a list of the four events arranged in order of increasing recorded amplitude at most of the five arrays. The event numbers refer to the events studied by Filson[1]. The data

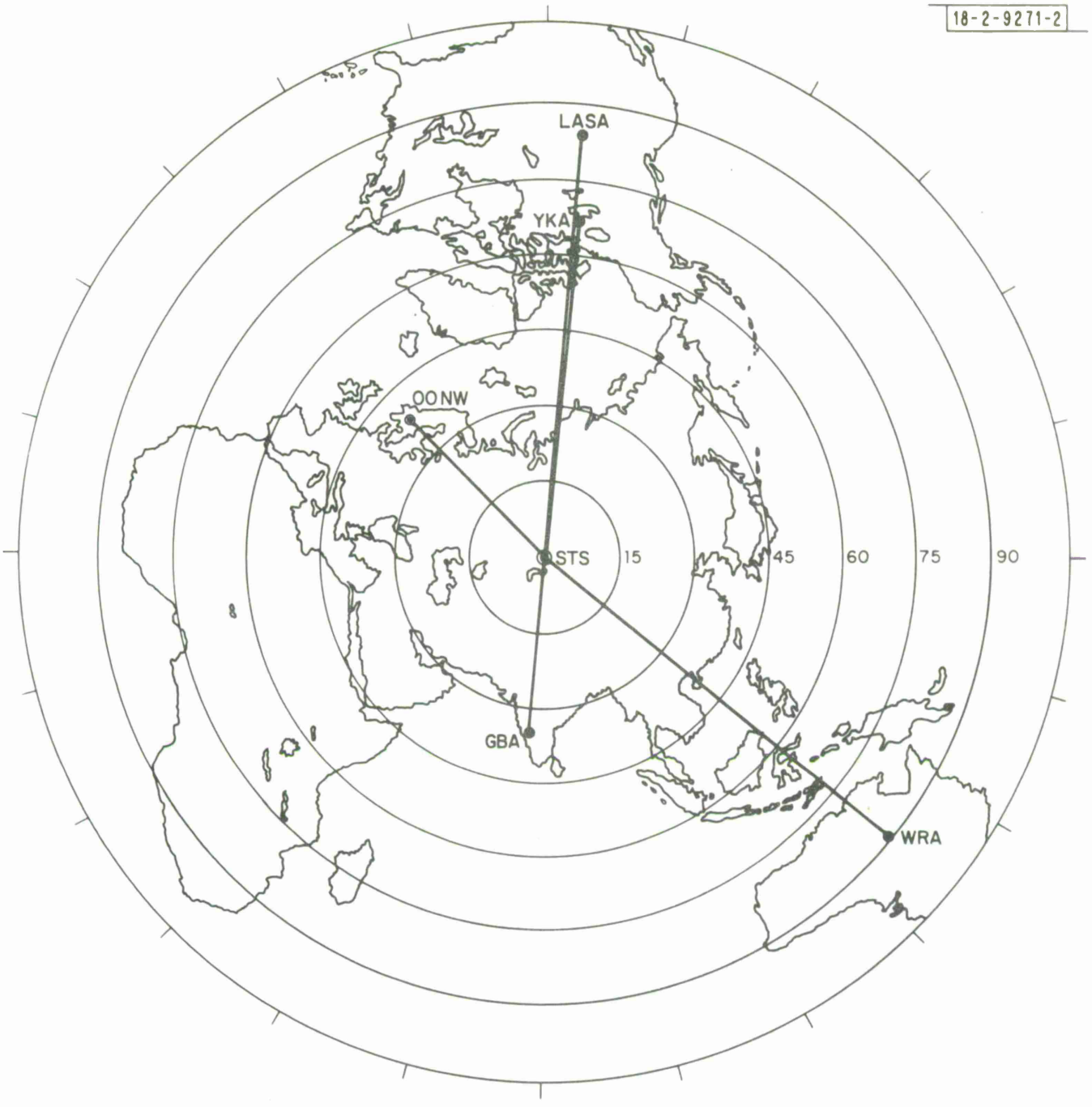

Fig. 1. World map showing the array locations relative to the Soviet test site (STS).

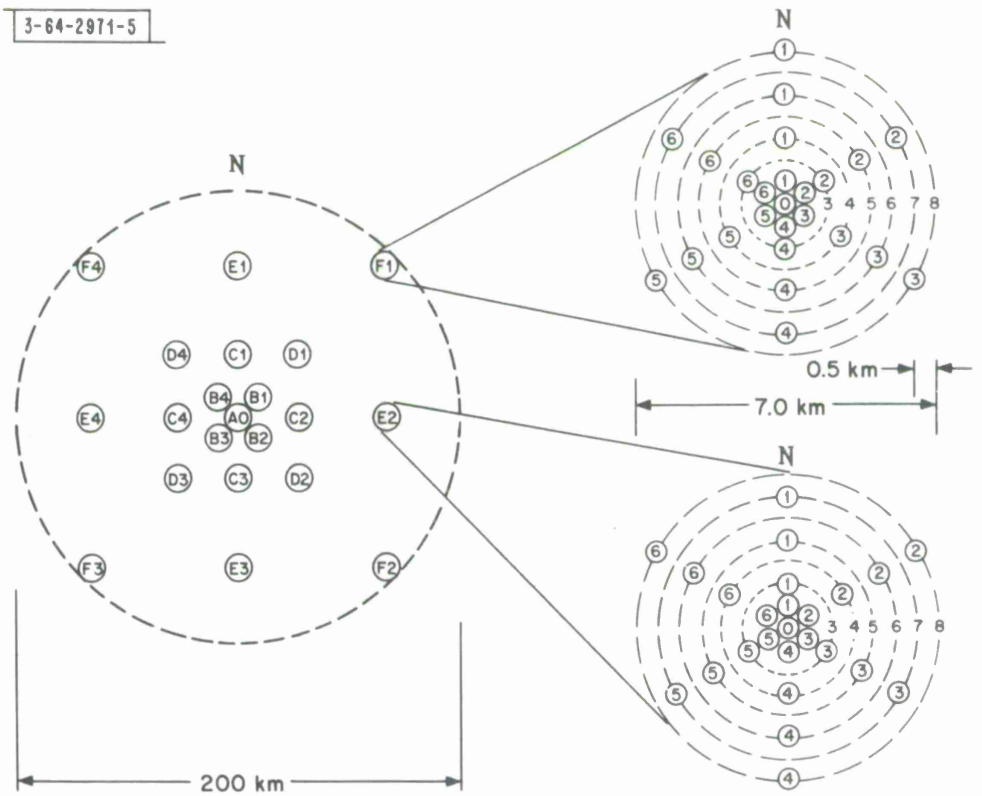

Fig. 2. LASA geometry. Center seismometer is at 46°41'19.0" N, 106°13'20.0" W.

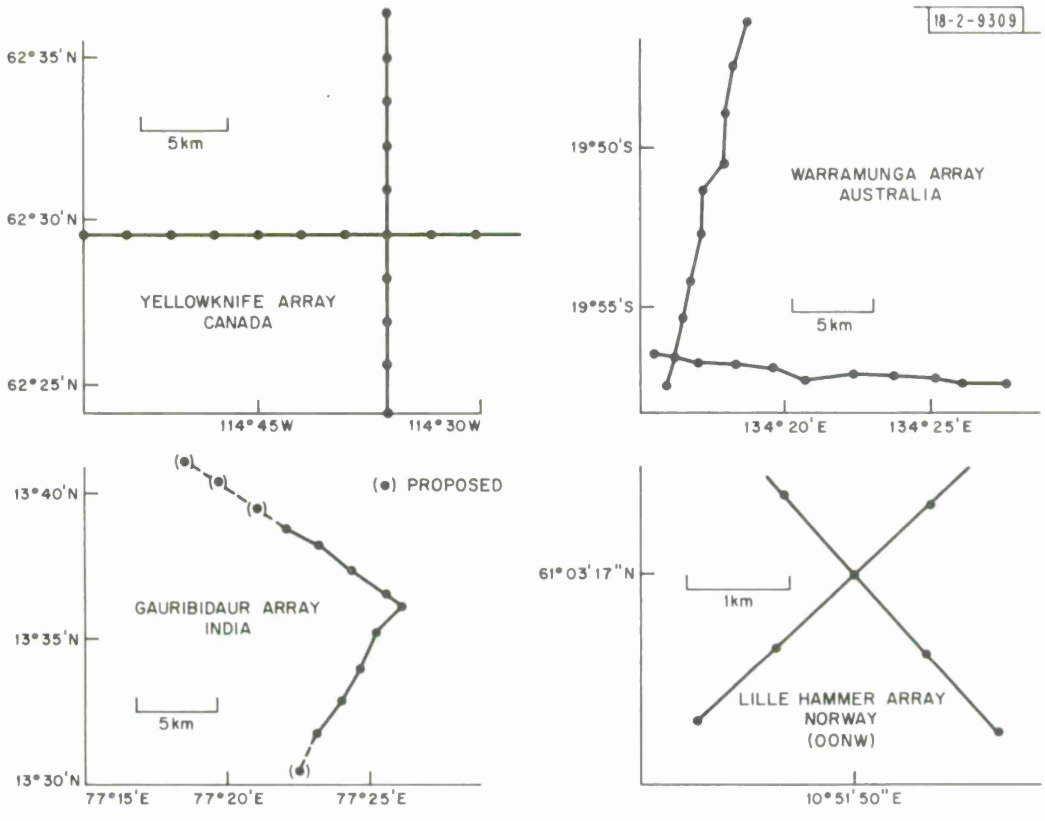

Fig. 3. Geometry of the United Kingdom arrays and OONW.

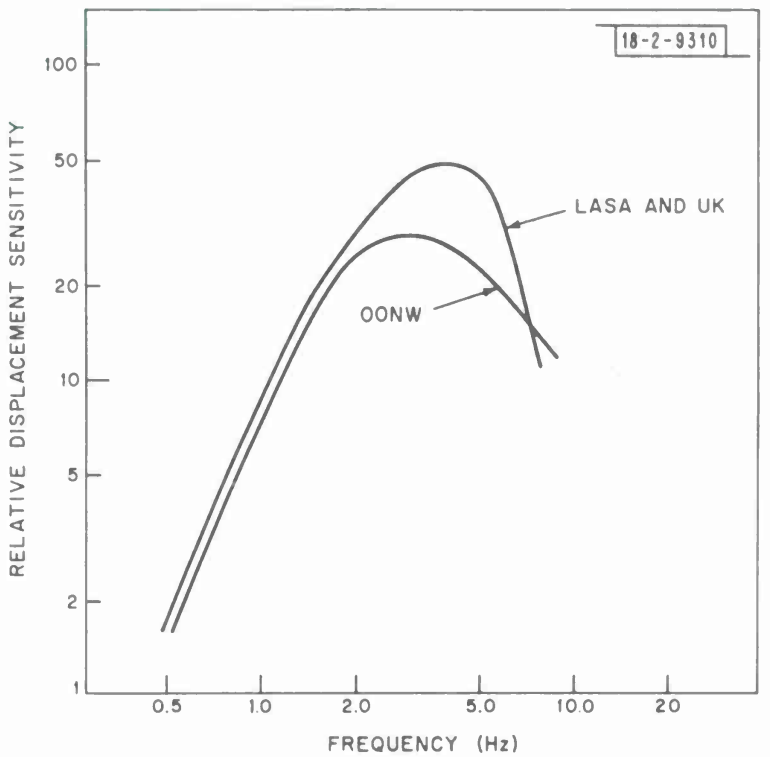

Fig. 4. Shapes of the response curves of the short period vertical instruments of the arrays.

tabulated without asterisks for Events 1, 2 and 5 were obtained from the Earthquake Data Report published by the USCGS. Event 4, however, was not reported by the USCGS. In order to locate this event relative to the other three, first motions were picked by the author at the LASA subarrays for all four events. For each event, a least squares plane wave was calculated for the subarray arrival times using the Analysis Console[2] at Lincoln Laboratory. The locations obtained are listed in the last column of Table 1.

Table 1

Event	M_b	Date	Origin Time			Location	Location (LASA)
			h	m	s		
1	5.3	Sept 22, '67	5	03	58	50.0N 77.6E	51.3N 79.9E*
2	5.3	Sept 16, '67	4	03	58	50.0N 77.8E	50.9N 78.4E*
4	---	Aug 4, '67*	6	57	58*		50.8N 78.1E*
5	5.7	Oct 17, '67	5	03	58	49.8N 78.1E	50.3N 78.4E*

Presumed Explosions from E. Kazakh. Data with asterisks(*) were estimated from LASA data by the author. Data without asterisks were obtained from the USCGS.

Figure 5 shows the USCGS and LASA locations of the events in Eastern Kazakh. As expected the LASA locations are not as tightly grouped as the USCGS locations. However, Event 4 appears to be located close to the other three events. For the purposes of this paper all events are assumed to have nearly identical epicenters.

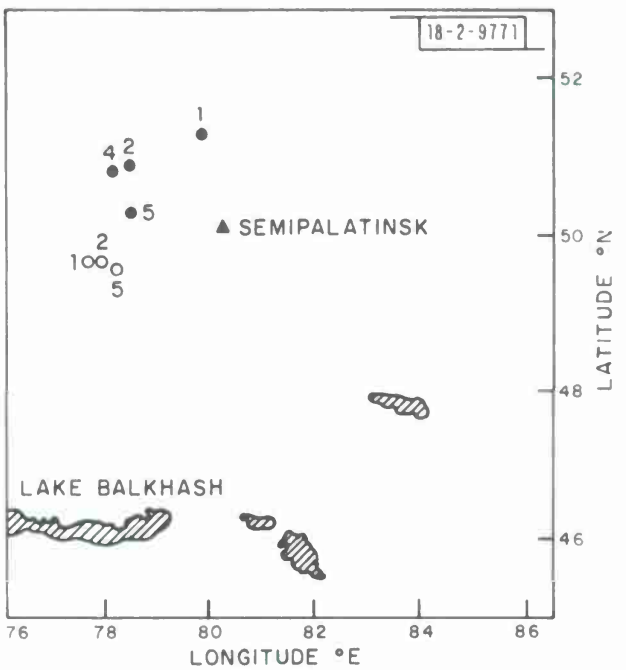

Fig. 5. Map of the Soviet test site region in Eastern Kazakh. Open circles are USCGS locations and solid circles are first motion LASA locations for the events studied.

III. CONSISTENCY OF SOURCE RADIATION TO EACH ARRAY

A crucial question is whether or not the observed seismic radiation is locally consistent over the aperture of each array. Figures 6 and 7 show seismograms from the largest and smallest arrays of this study, i.e. LASA and OONW. At LASA the subarray sum traces are shown and at OONW the individual seismometer traces are displayed. In each figure one can see considerable variation of signal shape and duration. These variations are not random however, but are quite repeatable from event to event at each site. This suggests that the teleseismic radiation arriving at each seismometer is severely altered by scattering in the crust and upper mantle under each recording site. At OONW Events 1 and 2 have identical shapes site for site, whereas Event 5 has a delayed phase, possibly a pP phase, which persists across all traces of the array. This delayed phase is not obvious at LASA nor at the other arrays.

In order to test the self-consistency of the data, transfer functions were first computed to shape Events 1, 2 and 4 to Event 5 at each sensor of the arrays. This is equivalent to computing the spectral ratio of two events in the frequency domain, including the phase information. Due to the tight cluster of epicenters, the transmission path effects from each source to a given receiver are assumed to be equal, thus dividing out in the frequency domain. This is a well known technique[3] for eliminating unknown but common transmission effects from pairs of signals. Such a spectral ratio should therefore equal the spectral ratio of the source radiations for the two events along the common take off direction from source to receiver. Unfortunately, each source radiation includes the depth of burial effect, which is an unknown factor mixed into the transfer functions of the data.

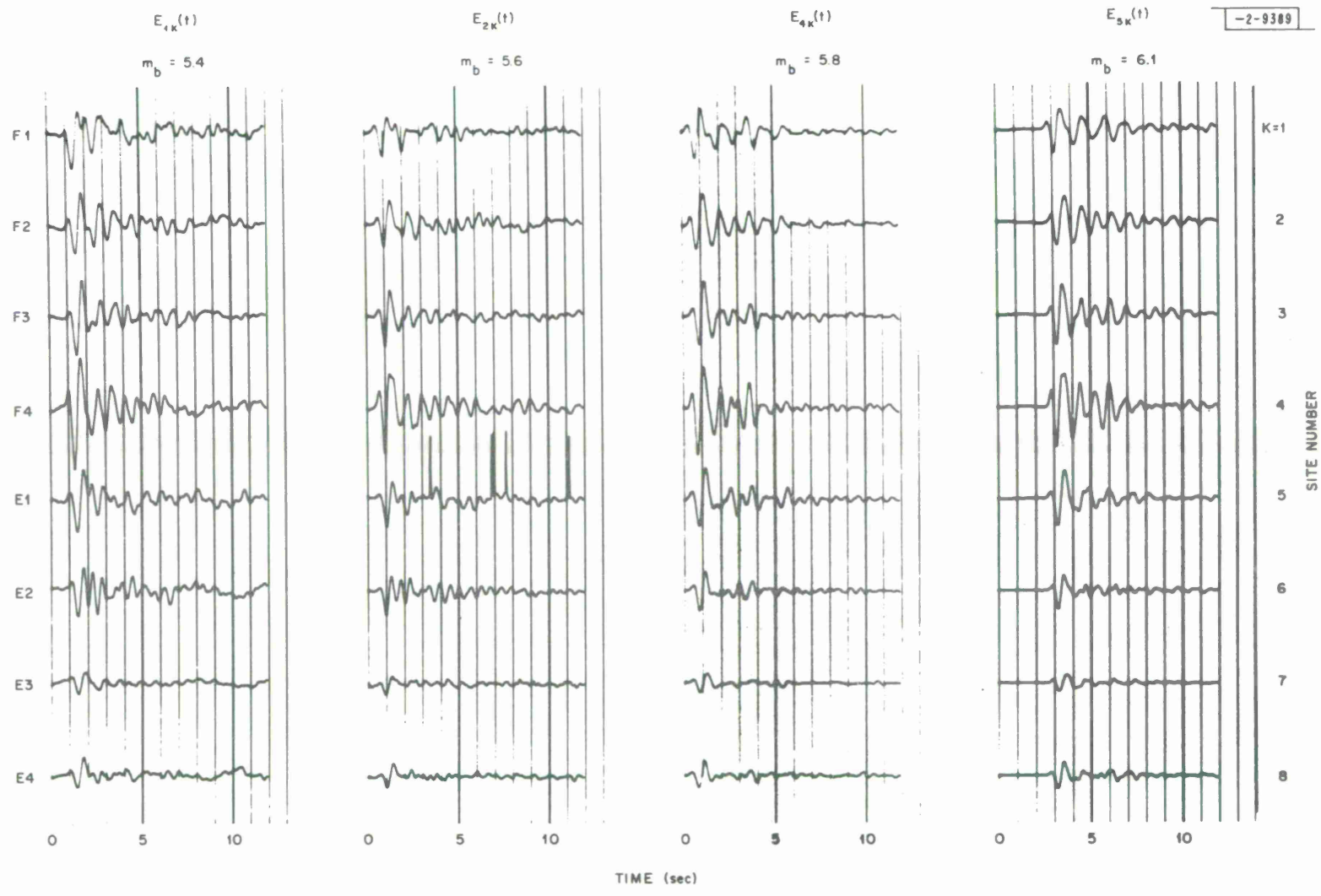

Fig. 6. LASA seismograms of the four events. They are arranged in order of increasing LASA magnitude from left to right. The relative amplitudes from subarray to subarray of each event are preserved.

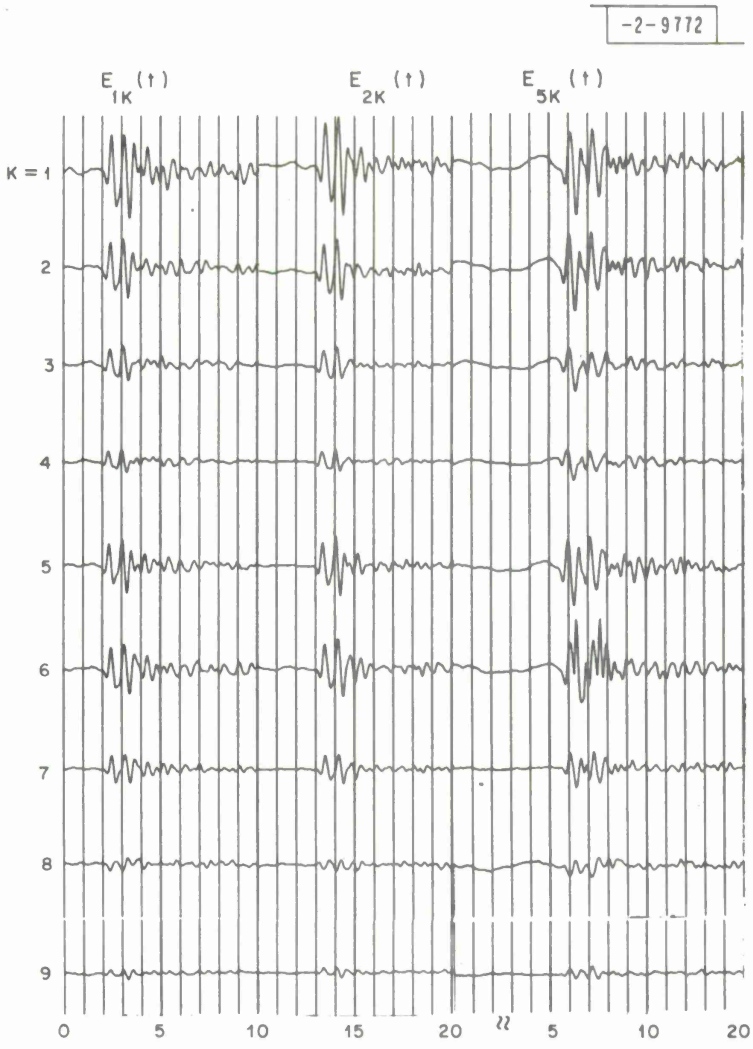

Fig. 7. OONW seismograms of three events. They are arranged in order of increasing amplitude from left to right. The relative amplitudes from sensor to sensor of each event are preserved.

If the source to receiver transmission effects are indeed common for events recorded at a given sensor, then sets of transfer functions, or spectral ratios, should be obtained which are locally consistent at LASA and at OONW in spite of the strong signal variations observed from sensor to sensor.

Let $E_{ik}(t)$ be the seismogram of Event i recorded at sensor k of either array. In the frequency domain we define the transfer function $R_{ijk}(\omega)$ as the ratio

$$R_{ijk}(\omega) = \frac{E_{ik}(\omega)}{E_{ik}(\omega)} \simeq \frac{S_i(\omega)}{S_i(\omega)} \qquad (1)$$

where $S_i(\omega)$ is the source spectrum of Event i along the take off angle to the array considered. Transfer functions were computed in time by a least squares method to shape each of the smaller events to Event 5, at the sites of each array. The sampling increments of the data is .05 sec. In each case a 50 point transfer function $R_{ijk}(t)$ was computed such that the convolution of 100 points of $E_{ik}(t)$ with $R_{ijk}(t)$ is the best least squares approximation to 149 points of $E_{jk}(t)$. This method is described in the Appendix.

Figures 8, 9 and 10 show the filters $R_{15k}(t)$, $R_{25k}(t)$ and $R_{45k}(t)$ respectively at LASA. Index k runs from 1 to 21 corresponding to the subarray sum traces at F1, F2, . . . E1, E2, . . . A0 respectively. In each figure the average filter $\overline{R}_{ij}(t)$ is also shown. The spike at the end of some filters is a spurious effect which should be ignored (see Appendix).

There is fairly good coherence of the transfer functions $R_{15k}(t)$ and $R_{25k}(t)$ from sensor to sensor despite the strong signal variations across LASA seen in Figure 8, and the transfer functions $R_{45k}(t)$ are extremely coherent.

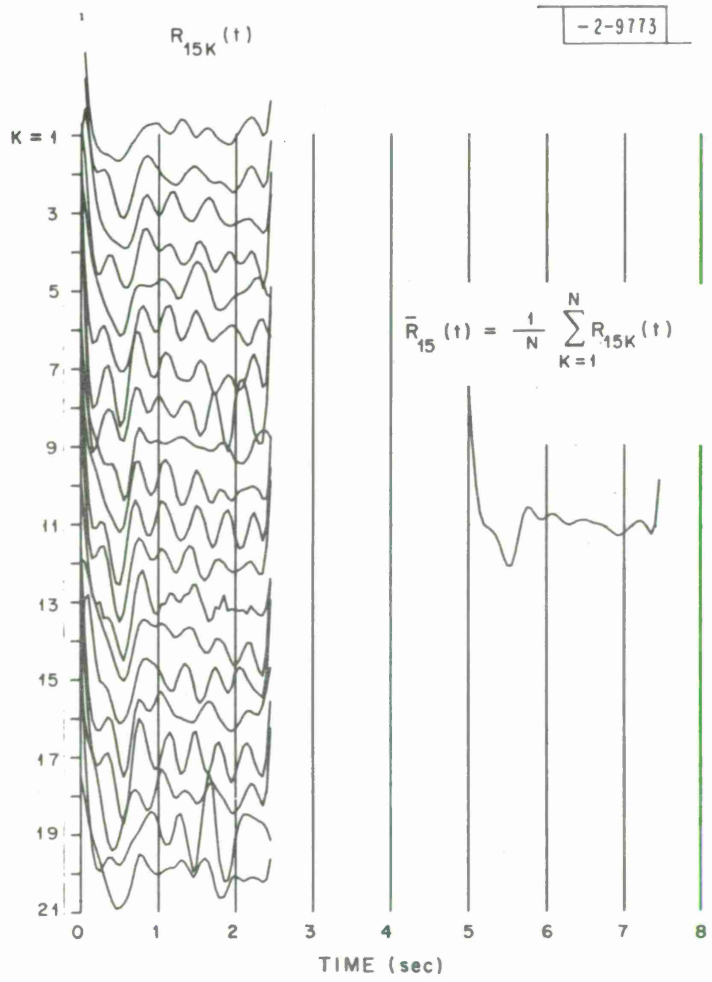

Fig. 8. Transfer functions $R_{15K}(t)$ at each available LASA subarray. The average filter $\bar{R}_{15}(t)$ is also displayed.

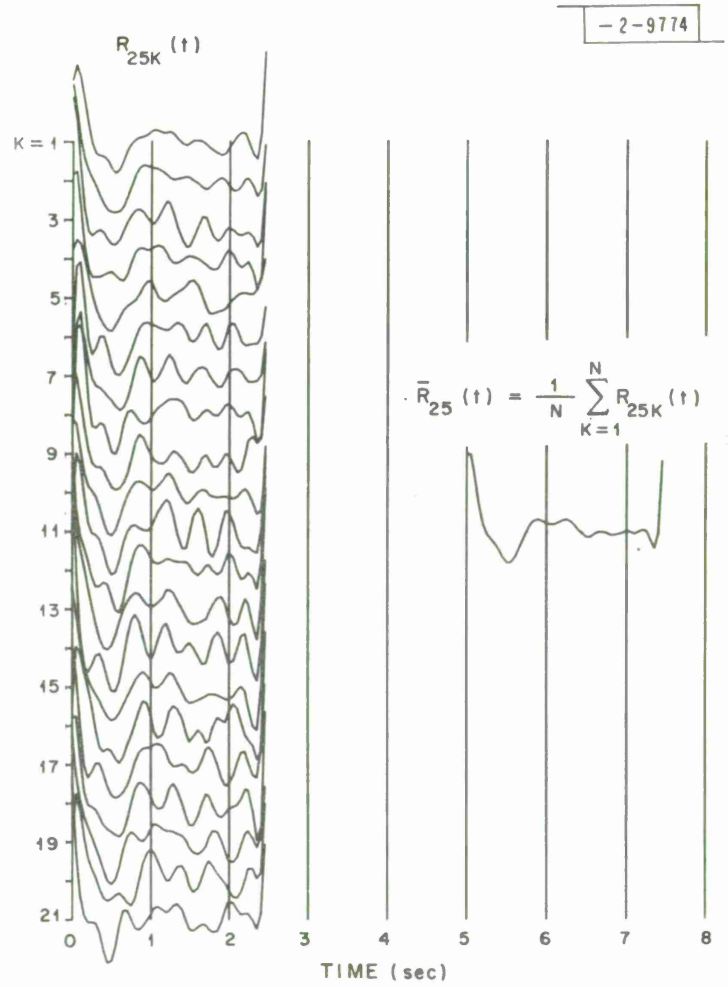

Fig. 9. Transfer functions $R_{25K}(t)$ at each available LASA subarray. The average filter $\bar{R}_{25}(t)$ is also shown.

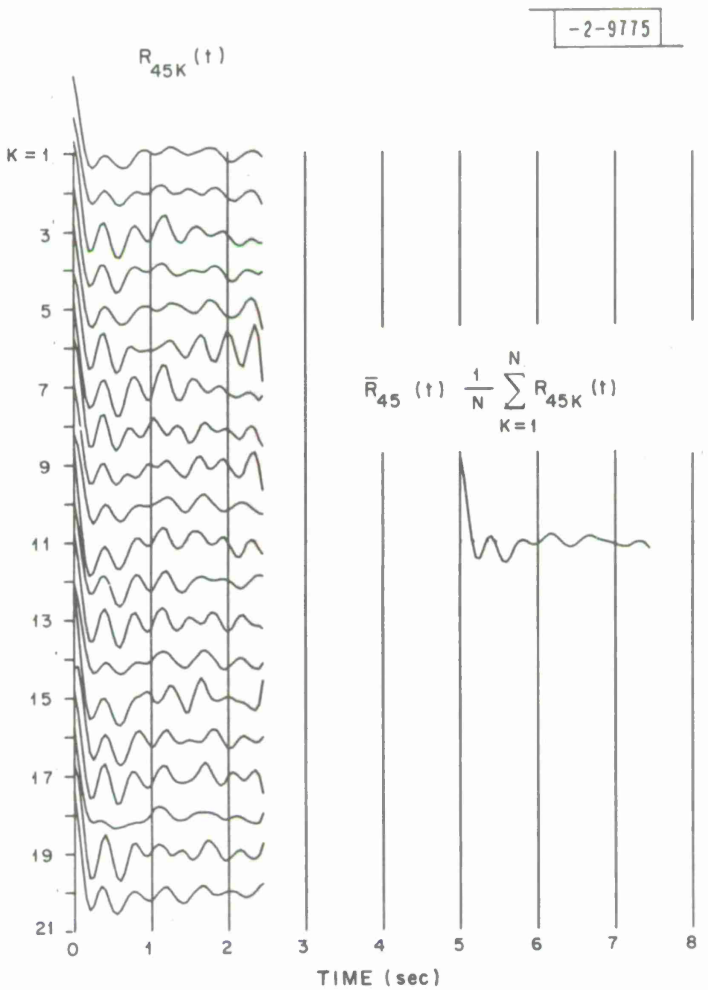

Fig. 10. Transfer functions $R_{45K}(t)$ at each available LASA subarray. The average filter $\bar{R}_{45}(t)$ is also shown.

In Figures 11 and 12 the transfer functions $R_{15_k}(t)$ and $R_{25_k}(t)$ are displayed for the available data at OONW. These transfer functions are also very coherent but are more oscillatory than the LASA transfer functions.

Similar calculations using the individual sensors of the United Kingdom arrays were done. Locally consistent transfer functions were also obtained at these arrays, although the signal to noise ratio of the data was not as good as the LASA data. From this one can conclude that variations in the source radiation of these events are not detected across the aperture of each array and that transmission path effects do cancel out. This implies that steered beams of each event can be used to calculate transfer functions without degrading source information.

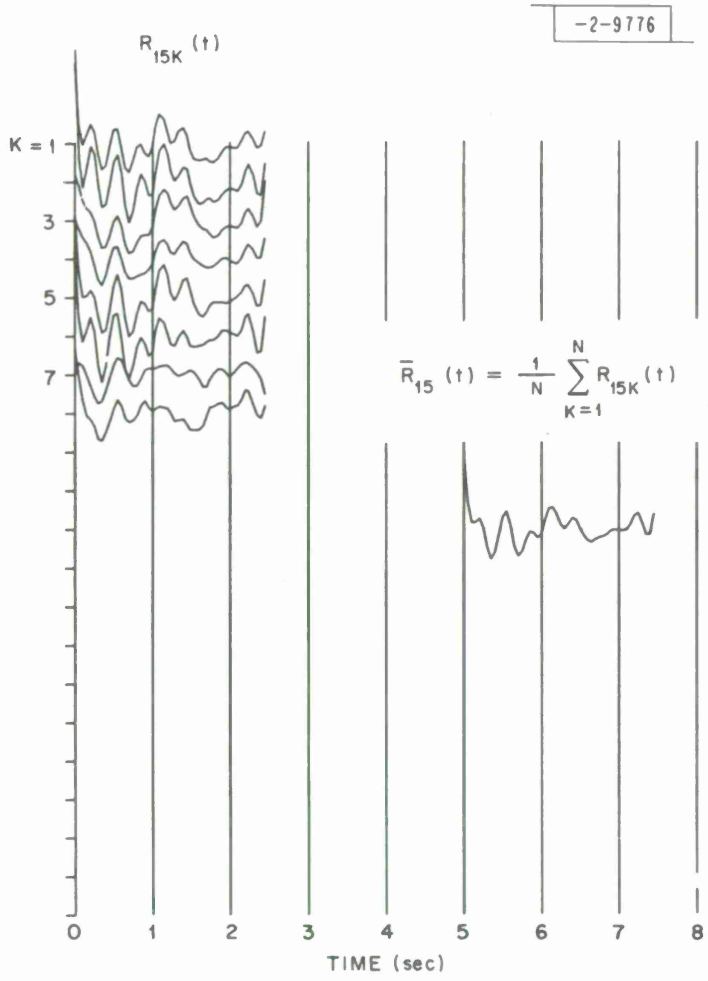

Fig. 11. Transfer functions $R_{15K}(t)$ at each available sensor at OONW. $\bar{R}_{15}(t)$ is the average filter.

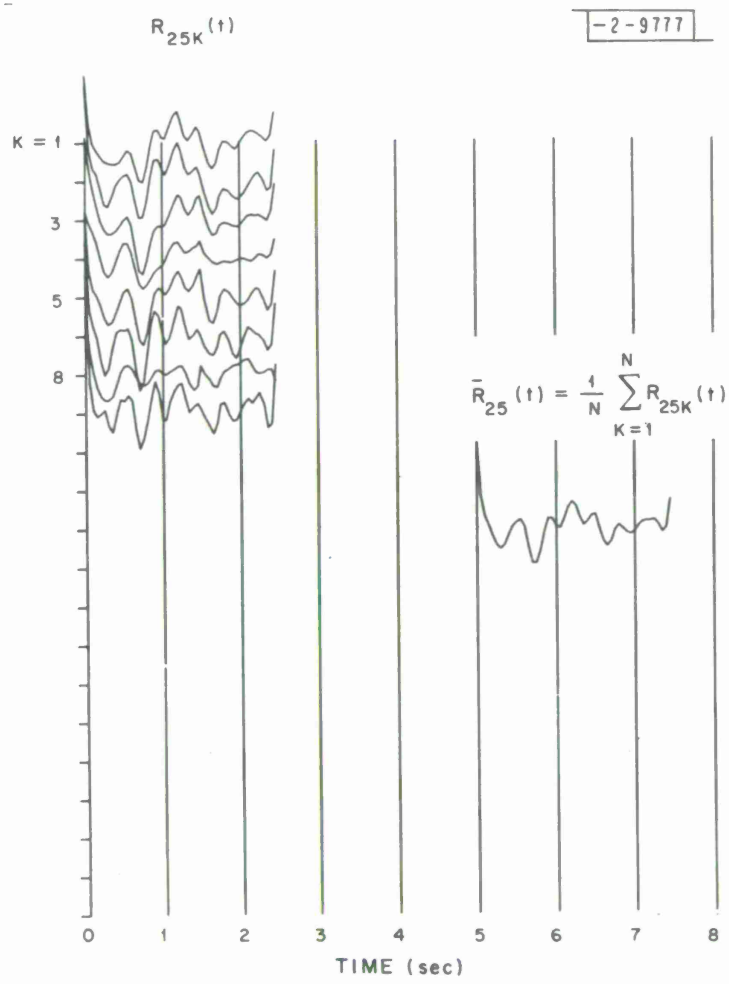

Fig. 12. Transfer functions $R_{25K}(t)$ at each available sensor at OONW. $\bar{R}_{25}(t)$ is the average filter.

IV. TRANSFER FUNCTIONS USING BEAM DATA

Figure 13 shows the steered beam traces at each array except LASA. At LASA the straight sum trace of the F3 subarray is shown in order to compare arrays of roughly the same size. Although there is some degradation of high frequencies in the straight sum trace[4], which could be removed by beam steering the individual traces, this degradation is common to all four events and will not affect the data analysis. Event 5 is normalized in Figure 6 to have the same trace amplitude at each array. The other three events are plotted with the correct amplitudes relative to Event 5. The local array magnitude for each event is indicated, those magnitudes with asterisks (*) being estimated by comparing amplitudes with other events at the same array. The instrument calibrations at the OONW array are unfortunately not known, but the relative amplitudes shown for the three events are considered reliable.

A glance at these beams shows that the seismic radiation patterns of the four events are not equal. At LASA, for example, there is a magnitude increase of .7 units from Event 1 to Event 5, whereas at GBA, Events 1 and 5 have the same magnitude. Another strange feature is the apparent discrepancy in radiation patterns recorded at LASA and YKA, although the take off angles and azimuths from the source region are nearly identical to both arrays. The precursors seen at YKA on Events 1 and 2, which are clearly seen on the individual sensors, are not present on Events 4 and 5. At LASA, no such precursors are seen on Events 1 and 2. At OONW an apparent depth phase occurs on Event 5 which is not seen on Events 1 and 2. Yet at GBA, which is the same distance from the Soviet Test Site but along a different azimuth, Events 5 and 1 are quite similar with no apparent depth phase seen.

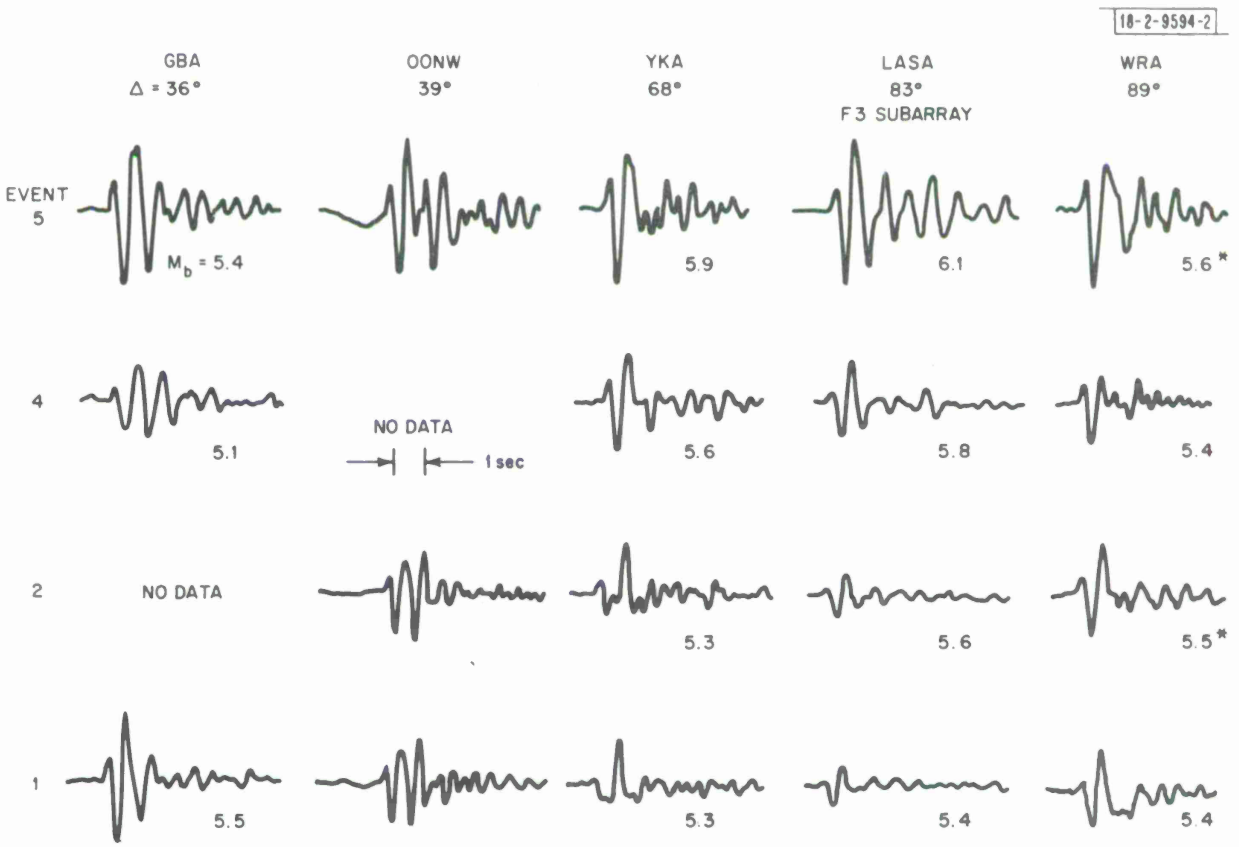

Fig. 13. Array beams of the four events. At LASA the straight sum for subarray F3 is shown. All other beams are steered.

These discrepancies in amplitude and wave shape are probably caused by site conditions which are difficult to separate. Small changes in epicenter and burial depth, the orientation of the initial stress field in the source region, and non-sphericity of the explosive pressure pulse are likely factors for producing anisotropic radiation to teleseismic distances.

Transfer functions $R_{15}(t)$, $R_{25}(t)$ and $R_{45}(t)$ were computed at each array using the beam data of Figure 13. These functions are displayed in Figure 14. If the seismic source radiations for each event were indeed isotropic, then the functions down each column would have the same shape and amplitude since transmission path effects have been eliminated. $R_{45}(t)$ seems to be consistent from array to array, whereas $R_{25}(t)$ and $R_{15}(t)$ increase in amplitude with epicentral distance from GBA to LASA, and then an amplitude drop to WRA. Thus Events 4 and 5 seem to have similar radiation patterns, however complex, but Events 1 and 5 clearly do not. The spikes at the end of some transfer functions should be ignored (see Appendix).

Of the five arrays YKA, LASA and WRA each have a complete set of three transfer functions. The numerical quality of the transfer functions is given by the normalized error e_N^2 described in the Appendix. $e_N^2 = 0$ indicates a perfect filter with no error, and $e_N^2 = 1$ is the worst case in which the least squares filter is zero. To illustrate this quality, Event 1 was convolved with $R_{15}(t)$ and compared with Event 5 at arrays YKA, LASA and WRA. These results are shown in Figure 15. Clearly, the convolution output for the YKA data is a poor approximation to Event 5, whereas at LASA the filtered data is in excellent agreement with Event 5. The normalized error e_N^2 is .38 at YKA, .06 at LASA and .17 at WRA. In Figure 14 all transfer functions, except those at YKA, perform as well or better than the WRA example shown in Figure 15.

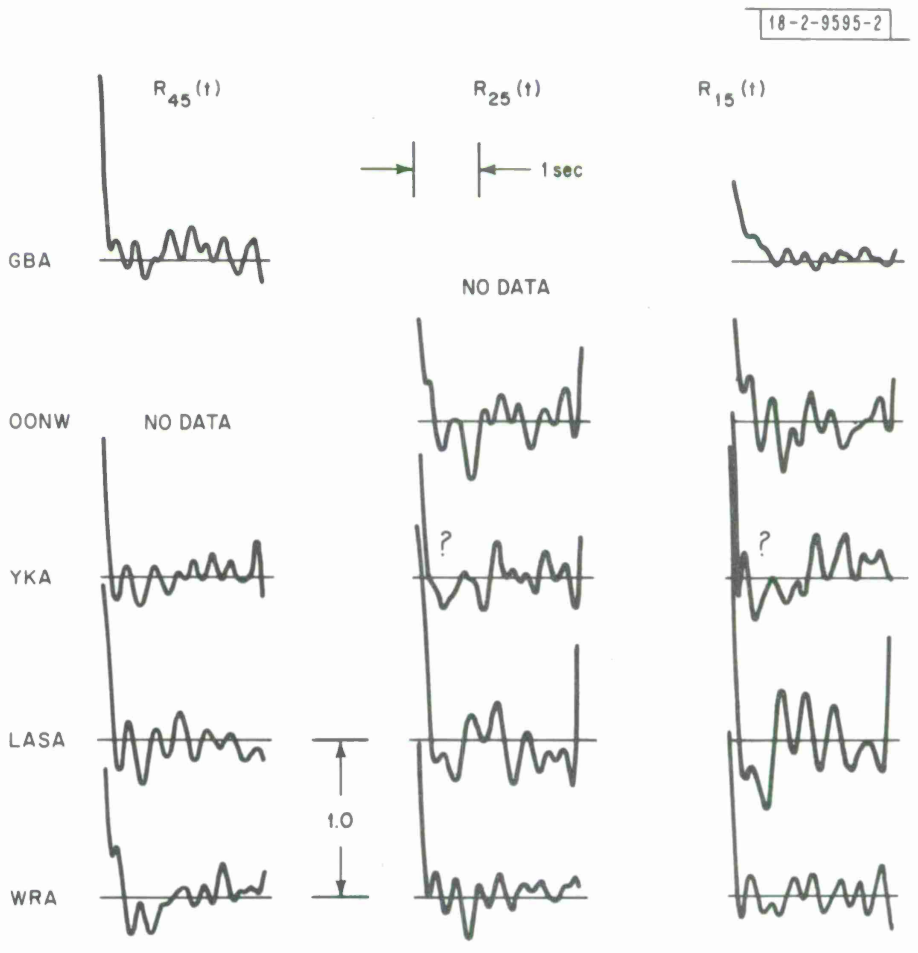

Fig. 14. Transfer functions $R_{i5}(t)$ at each available array for i = 1, 2, 4.

Fig. 15. Examples of numerical accuracy of computed transfer functions $R_{15}(t)$. In each column the middle trace is the convolution of Event 1 with $R_{15}(t)$, which can be compared with Event 5, the bottom trace. $R_{15}(t)$ at LASA is quite good, but the filter at YKA is poor quality.

V. THEORETICAL TRANSFER FUNCTIONS

In spite of the apparent anisotropy of the source radiations for the events studied, it is of interest to calculate theoretical transfer functions for assumed explosion models and see if such calculations match any trends in the observed LASA transfer functions, which were the most reliable, numerically.

Two isotropic mathematical models for the shape of compressional waves radiated from explosive sources are those of Blake[5] and Haskell[6]. Blake generalized a solution obtained by Sharpe[7] for P waves radiating from a cavity in an infinite homogeneous elastic medium, where the cavity is excited by a step function of pressure. Haskell took the near in displacement records of nuclear explosions from different media obtained by Werth and Herbst[8] and fit the record shape by a family of analytic functions which could be adjusted for different media and explosive yield.

Blake's expression for the far field radial particle velocity, $S_1(t)$, produced by applying a step function of pressure p_1 to an elastic cavity wall is

$$S_1(t) = \frac{p_1 a_1}{\rho c r} (2 - 2\sigma)^{\frac{1}{2}} e^{-\alpha_1 t} \cos(\omega_1 t + \phi) \qquad (2)$$

where

r = radial distance from source to receiver

c = compressional velocity of medium

σ = Poisson's ratio

ρ = density of medium

$$\alpha_1 = (c/a_1)\,(1 - 2\sigma)^{\frac{1}{2}}/(1 - \sigma)$$

$$\omega_1 = (c/a_1)\,(1 - 2\sigma)/(1 - \sigma) = (1 - 2\sigma)^{\frac{1}{2}}\alpha_1$$

and

$$\phi = \tan^{-1}(1 - 2\sigma)^{\frac{1}{2}}$$

For explosions the radius a is taken to be the equivalent elastic radius, outside of which the medium behaves elastically, whereas pressure p is determined by the lithostatic pressure at the test site. Both of these variables are functions of the burial depth which is not known for these events. As noted by Filson[1], cepstral analysis of these four events does not reveal consistent delay times at the five arrays for possible pP phases. We shall assume that all four events have equal depths in which case the pressures p_1 assumed for each elastic cavity are equal. For the computation of theoretical transfer functions for events recorded at the same site, it is sufficient to write the source function as

$$S_1(t) \sim a_1 e^{-\alpha_1 t} \cos(\omega_1 t + \phi) \tag{3}$$

where the tilda ($\sim$) denotes proportionality.

Another source model we shall consider is obtained from Haskell's reduced displacement potential ψ. In this case the far field radial particle velocity is given by

$$S_1(t) = \frac{1}{cr} \frac{d^2\psi_1(t)}{dt^2} ,$$

which for events recorded at the same site can be written

$$S_1(t) \sim \psi_1(\infty) k_1^2 e^{-k_1 t} \left[\frac{(k_1 t)^2}{2} (1 + 24B) - \frac{(k_1 t)^3}{6} (1 + 48B) + B(k_1 t)^4 \right] \quad (4)$$

The parameters $\psi(\infty)$, k and B were used by Haskell to generate a family of analytic functions $\psi(t)$ which would scale properly with yield Y (kilotons). For scaling purposes Haskell assumed that

$$\psi(\infty) \sim Y \quad (5)$$

$$k \sim Y^{-\frac{1}{3}} \quad (6)$$

and

$$a = 100\, Y^{\frac{1}{3}} \quad (7)$$

where a is the equivalent elastic radius in meters, from the source, outside of which the medium behaves elastically. This radius will be used in equation (3) for Blake's far field solution.

Under these gross assumptions the source function for either model, equation (3) or (4), has amplitude and time scales which are proportional to $Y^{\frac{1}{3}}$ at a given array. Yields are not available for these events; however, an approximate magnitude yield relationship can be assumed. The Soviet Test Site is within the northeastern edge of the Balkhash Chingiz Foldbelt, a region of intrusive igneous rocks overlain by folded sediments. We shall assume that the source medium for each shot is granite. For explosions in hard rock there is evidence[1,9] that body wave magnitude m_b up to about 6. can be approximated by the formula

$$m_b = 3.8 + \log_{10} Y \qquad (8)$$

This differs slightly from other magnitude yield relationships, e.g. those summarized by Marshall[10], but these differences are negligible for this analysis, considering the lack of consistency from array to array.

From the LASA body wave magnitudes a set of yields were calculated for the four events using equation (8). These are listed in Table 2. From these yields, values of $\psi(\infty)$ and k were computed from (5) and (6) by scaling up Haskell's values of $k = 31.6\ \text{sec}^{-1}$ and $\psi(\infty) = 2.5 \times 10^3 m^3$ for a 5 kt explosion in granite. These parameters and values of a_i calculated from (7) are also tabulated.

Table 2

Event	LASA m_b	Y_i	k_i	$\psi_i(\infty)$	a_i
1	5.4	39.8 kt	15.8 sec^{-1}	19.4 x $10^3 m^3$	341 m
2	5.6	63.0	13.6	31.5 x 10^3	398
4	5.8	100.	11.7	50.0 x 10^3	464
5	6.1	199.	9.16	100. x 10^3	584

Yield dependent parameters used in source functions for the events recorded at LASA.

The remaining parameters required for calculating the source functions are independent of yield, and depend on the source medium only. For Blake's far field

solution values of c = 5 km/sec, and $\tau = .3$ were assumed, and in Haskell's formula a value of the parameter B = .24 for granite was used.

From the above numbers source functions were calculated for each event using equations (3) and (4). These functions are shown in Figure 16. The main difference between the two source functions is that a step function of pressure in Blake's solution causes a discontinuity in the velocity response at zero time, whereas Haskell's analytical function was constrained to have continuous displacement, velocity, and acceleration at zero time.

Theoretical transfer functions $R_{15}(t)$, $R_{25}(t)$ and $R_{45}(t)$ were calculated for both sets of assumed source functions. These filters are superposed on the observed LASA transfer functions in Figure 17.

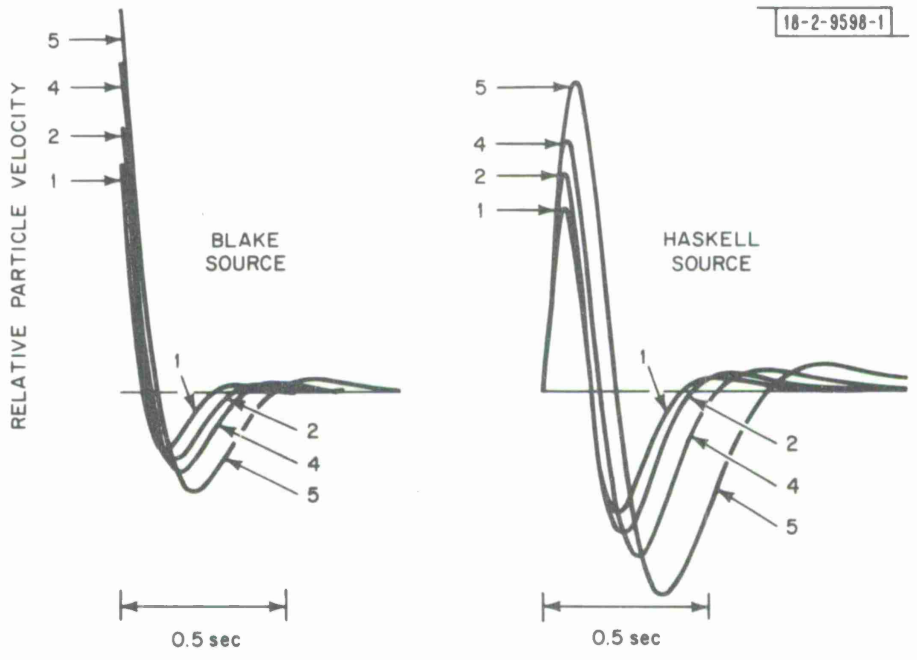

Fig. 16. Particle velocity source functions for the four events using Blake's and Haskell's model.

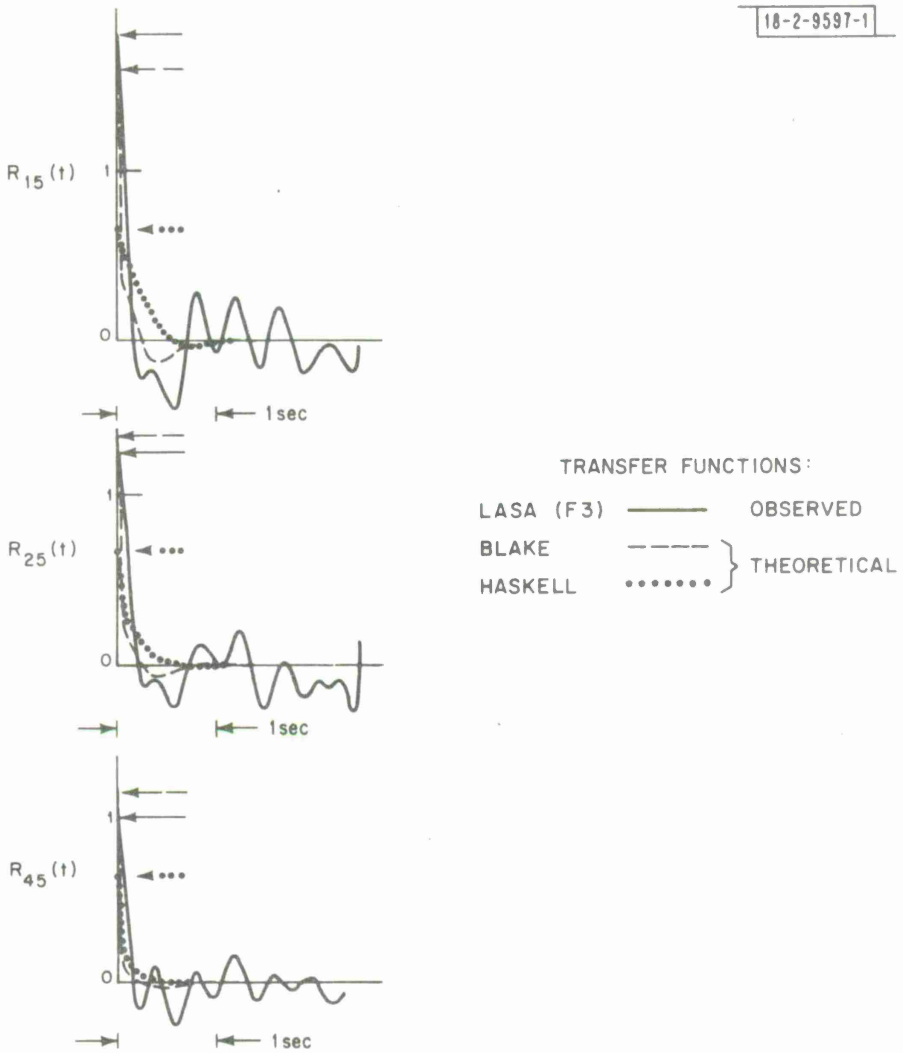

Fig. 17. Comparison of theoretical and observed transfer functions at LASA.

VI. DISCUSSION OF RESULTS AND CONCLUSIONS

From Figure 17 it appears that the transfer functions obtained from Blake's solution fit the observed LASA data better than those obtained from Haskell's source functions. Disregarding the 2-3 Hz oscillations, the first negative swing seen in $R_{15}(t)$ diminishes in $R_{25}(t)$ and $R_{45}(t)$ in both the data and the theoretical filters for Blake's source model.

Both source models predict a relative degradation of high frequencies with increasing magnitude. This implies that $R_{15}(\omega)$ should show a more rapid attenuation of high frequencies than either $R_{25}(\omega)$ or $R_{45}(\omega)$. This effect is demonstrated in Figure 18, which shows the amplitude spectra of the three LASA transfer functions. The curves have been normalized to unity at 1 Hz to emphasize the different attenuation rates of the filters.

A major drawback in this analysis is that the depth of focus of each event has been ignored. Unfortunately, the depth effect might contaminate that part of the transfer function which was interpreted in terms of scaled source functions. Taking the simplest example, let us assume that Event 1 was at zero depth, and Event 5 had a depth corresponding to a pP-P time of τ seconds. Then for identical point sources, the observed transfer function at teleseismic distance would be approximately

$$R_{15}(t) \sim \delta(t) + r\delta(t - \tau)$$

where r is the plane wave reflection coefficient at the free surface and $\delta(t)$ is the Dirac delta function. For any reasonable crustal model r varies from about -.7 to -1.0

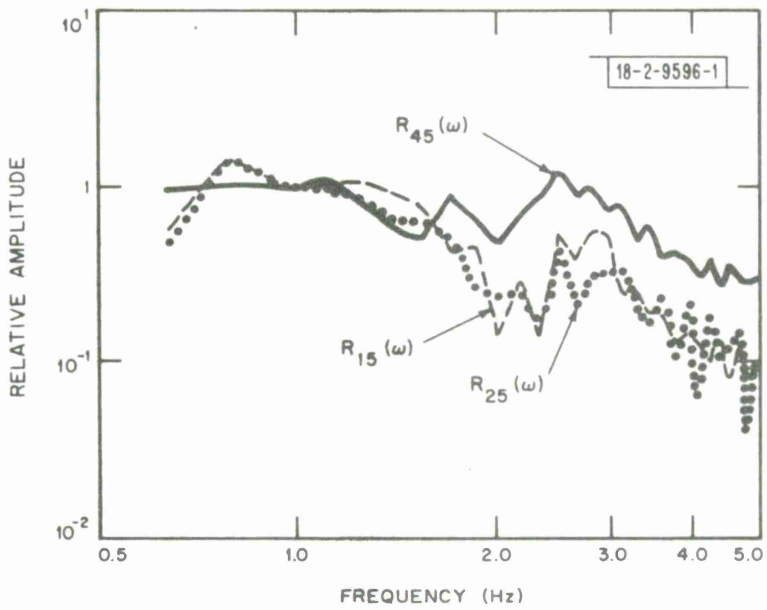

Fig. 18. Amplitude response of the LASA transfer functions. Curves are normalized to have amplitude 1 at 1 Hz.

depending on the take off angle from source to array. If τ is taken to be .5 sec., then $R_{15}(t)$ will consist of a positive spike followed by a smaller negative spike .5 sec. later. This operator, if band pass filtered, would have a shape similar to the first second of the LASA transfer function $R_{15}(t)$ shown in Figure 17.

The radiation of pP to teleseismic distances is obviously more complicated, as the data indicates. Numerical studies by Plamondon[11] show that strong multiple reflections occur between the free surface and a buried spherical cavity which has been excited by a pressure pulse. From this it follows that the observed teleseismic radiation from shallow cavities cannot be simply modelled by point sources. Clearly, numerical studies similar to those of Plamondon are needed to calculate the seismic radiation along different take off angles from well documented explosions. This may explain the observed anisotropy in source radiation and enable one to separate the effects of burial depth and seismic scaling.

ACKNOWLEDGEMENTS

The author benefitted from extensive discussions of the data with J. R. Filson. D. Davies and R. T. Lacoss critically reviewed this paper and made valuable suggestions. All this help is greatly appreciated.

APPENDIX

The method of least squares filters is very well known. One of the earliest and most readable references for practical computations using discrete time data is by Levinson[12]. This reference also appears as Appendix B of N. Wiener's book Time Series, M. I. T. Press, 1964.

One of the problems in the calculations of this paper is a spike which sporadically occurs at the ends of the transfer functions (or filters). This appears to be a function of the finite length data windows used in the filter calcuations. In order to discuss this it is necessary to examine the matrix equations used in the computations. To simplify the discussion let us consider the following small system of equations:

$$\begin{bmatrix} y_1 \\ y_2 \\ y_3 \\ y_4 \\ y_5 \\ y_6 \end{bmatrix} = \begin{bmatrix} x_1 & 0 & 0 \\ x_2 & x_1 & 0 \\ x_3 & x_2 & x_1 \\ x_4 & x_3 & x_2 \\ 0 & x_4 & x_3 \\ 0 & 0 & x_4 \end{bmatrix} \begin{bmatrix} f_1 \\ f_2 \\ f_3 \end{bmatrix} \tag{A1}$$

This equation gives the output, y_t, obtained by convolving the input data, x_t, with a filter f_t. For such a transient convolution the number of samples in y_t is one less than the sum of the filter and data lengths, i.e. $3 + 4 - 1 = 6$. Thus, if y_t and x_t are given, the system of equations is overdetermined for calculating f_t. However a solution for f_t can be obtained which minimizes the sum of squared errors between the desired output, y_t, and the actual convolution.

If we write (A1) in the following matrix notation

$$\bar{y} = \bar{\bar{X}}\bar{f}\,, \tag{A2}$$

then premultiplying (A1) by $\bar{\bar{X}}^T$ gives

$$\bar{\bar{X}}^T\bar{\bar{X}}\bar{f} = \bar{\bar{X}}^T\bar{y} \tag{A3}$$

where
$$\bar{\bar{X}}^T\bar{\bar{X}} = \begin{bmatrix} r_0 & r_1 & r_2 \\ r_1 & r_0 & r_1 \\ r_2 & r_1 & r_0 \end{bmatrix} = \bar{\bar{R}}\,,$$

and
$$r_\tau = \sum_{i=1}^{4-i+1} x_i x_{i+\tau}\,, \quad \tau = 0, 1, 2. \tag{A4}$$

The solution for $\bar{f}$ in (A3) is the least squares solution of (A1). $\bar{\bar{R}}$ is a positive definite matrix and each element r_τ is the transient autocorrelation of the input data x_t at lag τ. The elements along any diagonal of $\bar{\bar{R}}$ are equal, hence $\bar{\bar{R}}$ is called a Toeplitz matrix. Large matrices of this form can be inverted very rapidly using Levinson's algorithm[13].

Referring to Section IV of this paper we let x_t be $E_1(t)$, and y_t be $E_5(t)$ so that f_t corresponds to the transfer function $R_{15}(t)$ computed at one of the arrays. In order to apply an equation like (A1) to real data, $E_1(t)$ and $E_2(t)$ must be truncated even though it is often not clear when a P wave terminates. From equation (A1) one sees that y_5 and y_6 are not functions of x_5 and x_6 because only four points of x_t were used. This may introduce numerical errors into f_2 and f_3 which are physically not meaningful.

One possible test of the sensitivity of f_2 and f_3 to this data is to set $y_5 = y_6 = 0$ in (A1). This will have no effect on f_1, but may change f_2 and f_3 significantly.

This idea was checked for a large system of equations similar to (A1) using $E_1(t)$ and $E_5(t)$ recorded at LASA. In Figure 19 results of a filter calculation are shown using 60 samples of $E_1(t)$ as input, and 109 points of $E_5(t)$ as desired output. A least squares transfer function 50 samples long was computed. This filter shows a large positive spike at the end.

In Figure 20 the same length filter was computed, but in this case all samples of $E_5(t)$ past number 60 were arbitrarily set equal to zero. In this case the spike at the end of the filter has been removed, but the early part of the filter remains unchanged. The convolution of the filter with the input data yields a good approximation to the desired output, even for the zeroed portion of the data.

The error minimized in designing the filter is the sum of squares

$$e^2 = (\bar{y} - \bar{\bar{X}}\bar{f})^T (\bar{y} - \bar{\bar{X}}\bar{f}) \tag{A5}$$

Using (A3), this reduces to

$$e^2 = \bar{y}^T\bar{y} - \bar{f}^T\bar{\bar{X}}\bar{\bar{X}}\bar{f} \tag{A6}$$

Dividing e^2 by the sum of squares $\bar{y}^T\bar{y}$ we obtain the normalized error

$$e_N^2 = 1 - \bar{f}^T\bar{\bar{X}}\bar{\bar{X}}\bar{f} \tag{A7}$$

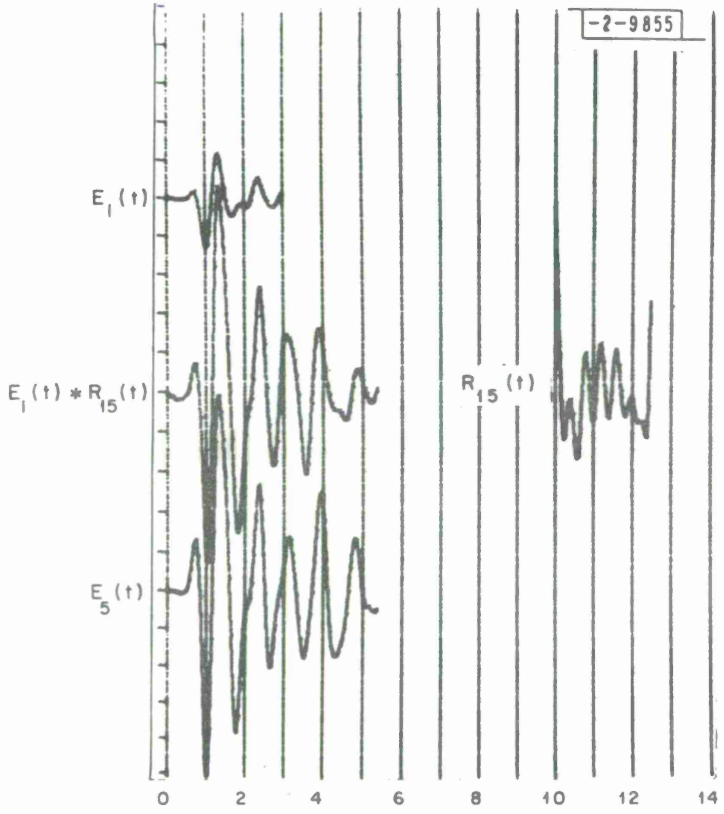

Fig. 19. Transfer function $R_{15}(t)$ at LASA computed using 60 points of $E_1(t)$ and 109 points of $E_5(t)$. The convolution $E_1(t)*R_{15}(t)$ is a good approximation to $E_5(t)$.

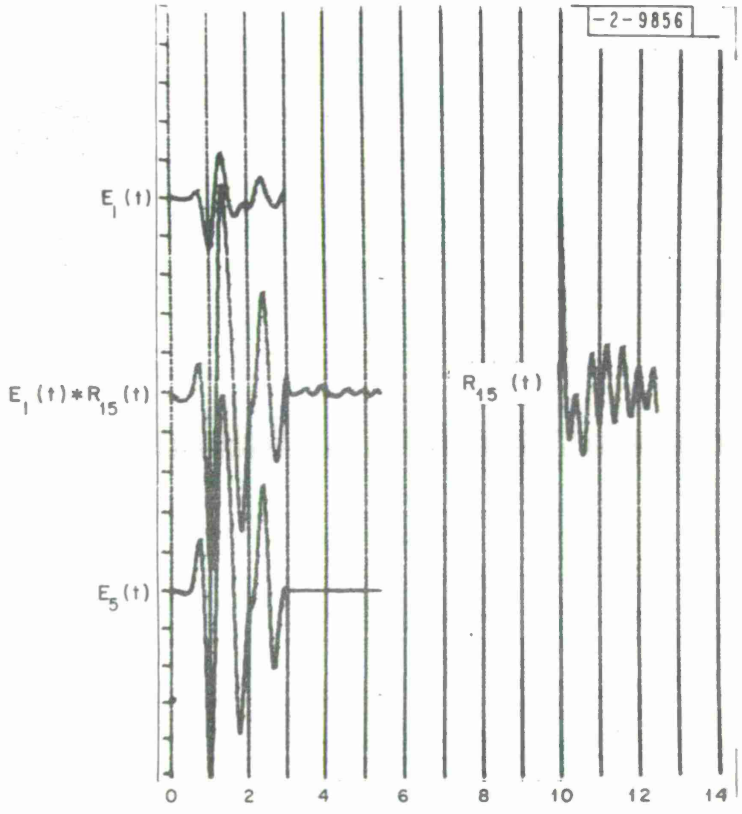

Fig. 20. Transfer function $R_{15}(t)$ computed as in Fig. 19 but with only 60 points of $E_5(t)$ being used. $R_{15}(t)$ shows no spike at the end in this case.

which falls in the range 0 to 1. If $e_N^2 = 0$, the filter exactly converts x_t to y_t, and if $e_N^2 = 1$, the filter does the poorest job of shaping x_t to y_t. This occurs when x_t and y_t are uncorrelated and all f_t are zero.

The filters computed at LASA, for example, all have normalized errors of < 0.1. At the other arrays the filters have normalized errors as large as 0.3.

The analysis in this paper of the LASA filters in terms of source functions was pertinent only to the first 20 points (1 second) of the filters. These filter points are numerically stable and show very little dependence on the length of x_t, y_t or f_t specified in the calculations, as long as f_t has more than about 30 points.

The effect of the convolution "tail" in (A1) can be eliminated by using the same number of samples in x_t and y_t. This can be done by taking only the first four equations of (A1), for example, and repeating the analysis through (A7). The only difficulty in this case is that $\bar{\bar{R}}$ is no longer a Toeplitz matrix and is considerably more time-consuming to invert.

References

1. Filson, J. R., "On Estimating Explosive Source Parameters at Teleseismic Distances," Technical Note 1970-9, Lincoln Laboratory, M. I. T. (8 July 1970).

2. Fleck, P., "A Seismic Data Analysis Console," Technical Note 1968-14, Lincoln Laboratory, M. I. T. (19 June 1968).

3. Teng, Ta-Liang, "Attentuation of Body Waves and the Q Structure of the Mantle," J. Geophys. Res. 73, 2195-2208 (1968).

4. Lacoss, R. T., Kuster, G. R., "Processing a Partially Coherent Large Seismic Array for Discrimination," Technical Note 1970-30, Lincoln Laboratory, M. I. T. (27 November 1970).

5. Blake, F. G., "Spherical Wave Propagation in Solid Media," J. Acoust. Soc. Amer. 24, 211-215 (1951).

6. Haskell, N. A., "Analytic Approximation for Elastic Radiation from a Contained Underground Explosion," J. Geophys. Res. 72, 2583-2587 (1969).

7. Sharpe, J. A., "The Production of Seismic Waves by Explosion Pressures. I. Theory and Empirical Field Observations," Geophysics 18, 144-154 (1942).

8. Werth, G. and Herbst, R., "Comparison of Amplitudes of Seismic Waves from Nuclear Explosions in Four Mediums," J. Geophys. Res. 68, 1463-1475 (1963).

9. Davies, D. (rapporteur), "Seismic Methods for Monitoring Underground Explosions," published by SIPRI, Stockholm (1968).

10. Marshall, P. D., "Aspects of the Spectral Differences Between Earthquakes and Underground Explosions," Geophys. J. R. Astr. Soc. 20, 397-416 (1970).

11. Plamondon, M. A., "Reflection of Spherical Elastic Stress Waves from a Plane Surface," Ph. D. Thesis, University of Illinois (1966).

12. Levinson, N., "The Wiener RMS (Root Mean Square) Error Criterion in Filter Design and Prediction," J. Math. and Phys. 25, 261-278 (1947).

DOCUMENT CONTROL DATA – R&D

(Security classification of title, body of abstract and indexing annotation must be entered when the overall report is classified)

1. ORIGINATING ACTIVITY *(Corporate author)*
Lincoln Laboratory, M.I.T.

2a. REPORT SECURITY CLASSIFICATION
Unclassified

2b. GROUP
None

3. REPORT TITLE
Seismic Scaling of Explosive Source Functions Using Teleseismic P Waves

4. DESCRIPTIVE NOTES *(Type of report and inclusive dates)*
Technical Note

5. AUTHOR(S) *(Last name, first name, initial)*
Frasier, Clint W.

6. REPORT DATE	7a. TOTAL NO. OF PAGES	7b. NO. OF REFS
14 April 1971	42	12

8a. CONTRACT OR GRANT NO. F19628-70-C-0230

b. PROJECT NO. ARPA Order 512

c.

d.

9a. ORIGINATOR'S REPORT NUMBER(S)
Technical Note 1971-11

9b. OTHER REPORT NO(S) *(Any other numbers that may be assigned this report)*
ESD-TR-71-116

10. AVAILABILITY/LIMITATION NOTICES
Approved for public release; distribution unlimited.

11. SUPPLEMENTARY NOTES
None

12. SPONSORING MILITARY ACTIVITY
Advanced Research Projects Agency, Department of Defense

13. ABSTRACT

Short period P waves of four presumed Soviet explosions from Eastern Kazakh are examined at five teleseismic arrays: LASA, YKA, OONW, WRA and GBA. Transfer functions to shape the lower magnitude to the highest magnitude event were computed at each array to eliminate transmission path effects from source to receiver. The transfer functions are locally consistent from sensor to sensor at each array, but show considerable global variations from array to array. This suggests that there are strong azimuthal variations in the source radiation of the events, due to complex scattering of the signals at the test site. At LASA, the observed transfer functions can be explained by using explosion source functions of Blake and Haskell. The assumed source parameters are scaled functions of the yield of each event, which is estimated from an empirical amplitude yield relationship.

14. KEY WORDS

LASA
seismic discrimination
seismometers
sensors
teleseismic arrays
transfer functions
P waves
source functions